Electrochemical template synthesis of protein-imprinted magnetic polymer microrods

Giorgio Ceolin · Ágnes Orbán · Vilmos Kocsis · Róbert E. Gyurcsányi · István Kézsmárki · Viola Horváth

Abstract A novel method for the electrochemical template synthesis of surface-imprinted magnetic polymer microrods for protein recognition is proposed. The polymer was electrodeposited into sacrificial cylindrical microreactors, the internal walls of which were previously modified with a target model protein, avidin, by simple physisorption. The electropolymerization was performed from a mixture of 3,4-ethylenedioxythiophene, poly(styrenesulfonate) (PSS), and PSS-coated superparamagnetic nanoparticles resulting in the formation of inherently electroconductive polymers confined to the volume of the microreactor. Here we show that: (i) the template synthesis within cylindrical microreactors results in polymer rods with dimensions matching that of the reactor, (ii) the incorporation of superparamagnetic particles induces magnetic properties that allow for efficient collection and manipulation of the microrods released from the microreactors in magnetic field even from dilute solution, and (iii) the protein coating on the internal walls of the microreactors is shown to generate molecular imprints on the surface of the polymeric rods. This latter property was demonstrated by comparative binding experiments of a fluorescent avidin derivative to the surface-imprinted and non-imprinted magnetic polymer microrods.

G. Ceolin · R. E. Gyurcsányi
Department of Inorganic and Analytical Chemistry, Budapest University of Technology and Economics, Szt. Gellért tér 4., Budapest 1111, Hungary

Á. Orbán · V. Kocsis · I. Kézsmárki
Department of Physics, Budapest University of Technology and Economics and Condensed Matter Research Group of the Hungarian Academy of Sciences, Budafoki út 8., Budapest 1111, Hungary

R. E. Gyurcsányi · V. Horváth (✉)
MTA-BME Research Group of Technical Analytical Chemistry, Hungarian Academy of Sciences, Budapest University of Technology and Economics, Szt. Gellért tér 4., Budapest 1111, Hungary
e-mail: vhorvath@mail.bme.hu

Introduction

Molecular imprinting is a general method to create selective recognition sites in synthetic materials, primarily polymers [1–4]. The imprinting is performed by polymerizing properly selected functional monomers in the presence of a target species, which acts as a molecular template. Thus, removal of the target after polymerization leaves behind binding sites complementary in size and functionality with the target enabling their preferential rebinding. Such materials with "molecular memory" were found to be useful in a wide range of applications as selective sorbents [5, 6], catalysts [7], selective sensing materials [8–10], etc. In spite of many successful applications and with products on the market MIPs are still facing major challenges, especially when switching from low molecular weight targets to biomacromolecules such as proteins [11]. The large molecular size induces mass transport limitations for removal and rebinding in the three-dimensional polymer network. Other complication may arise from conformational changes of the biomacromolecules and cross reactivity due to the large number of functionalities.

The most promising direction to overcome difficulties in the template removal and rebinding is surface imprinting, which generates binding sites exclusively on the surface of the imprinted material. This can be accomplished on planar surfaces or on the surface of nano- or microparticles. The

first format is preferred for sensing applications where the MIP layer is deposited on a suitable electrochemical, piezoelectric, or surface plasmon resonance-based transducer. The second format, namely the surface-imprinted nanoparticles offer the possibility of using such materials for a wider range of applications involving cleanup, separation, and sensing, with clear benefits in terms of faster binding kinetics experienced in general on micro- and nanoparticulate reagents as compared with planar surfaces. However, handling of micro- and nanoparticles becomes difficult in heterogeneous assays with classical filtration, dialysis, or centrifugation separation methodologies. Clearly the most advantageous approach would be to impart superparamagnetic properties to nanoparticle MIPs. Therefore, magnetic MIP nano/microparticles have a promising perspective in heterogeneous bioassays because their stability and selectivity are conjugated with the ease of separation from the unbound analyte by magnetic field gradient [12]. Two general approaches to functionalize magnetic nanoparticles with molecularly imprinted polymers emerged: (i) the surface of the particles is modified with a thin layer of polymer (core–shell particles) or (ii) the magnetic nanoparticles (MNP) are dispersed in the polymeric matrix (multicore particles).

Different polymerization methods can be used to achieve the above-mentioned morphologies. Suspension and emulsion polymerization and the variations thereof [13–26] usually create multicore polymeric beads with embedded magnetic nanoparticles. These methods require a good synthetic skill to obtain uniform particles with appropriate morphology. Possible problems are leakage of magnetic particles from the beads especially at low pH values, low incorporation efficiency resulting in low magnetization [13], and unfavorable optical properties due to surface-bound magnetite [27].

The growth a thin MIP layer on the surface of the magnetic nanoparticle results in core–shell magnetic MIPs. As a consequence of the procedure the magnet is fully encapsulated by the thin imprinted polymer layer, thereby leading to high incorporation efficiency [28–37].

While all these techniques are based on chemical polymerization, we have recently introduced new strategies to surface imprint electrosynthesized electrically conducting polymers with biomacromolecules [38, 39]. These are based on sacrificial template synthesis using various geometry microreactors with their inner wall modified with the target protein to generate surface-imprinted polymers. Our effort was directed to synthesize surface-grafted microstructures for selective recognition of proteins largely benefiting from the advantages of well-controlled electropolymerization reactions that enabled the precise confinement of the structures to the volume of the microreactors. Owing to the wider applicability of surface-imprinted nano- and microparticles here we explored the feasibility of downscaling the procedure to generate smaller microparticles in solution phase imparting them with superparamagnetic properties for easy handling. Accordingly we are reporting for the first time the synthesis of surface-imprinted magnetic nanoparticles prepared by electropolymerization for protein recognition.

Experimental

Materials

Disk-shaped hydrophobic PVPF (polyvinylpyrrolidone free) track-etched polycarbonate membranes (PC membranes) with pore diameters of 1 and 0.1 μm, respectively, were purchased from GE Water & Process Technologies (Trevose, PA, USA). Poly(sodium 4-styrene-sulfonate) (PSS, MW ~ 70,000), 3,4-ethylenedioxythiophene (EDOT), avidin (Av, MW 68,000), fluorescein isothiocyanate-labeled avidin (avidin-FITC), and bovine serum albumin (BSA, MW 67,000) were purchased from Sigma-Aldrich (St. Louis, MO, USA). FluidMAG-PS magnetic nanoparticles (25 mg/mL) with magnetite core and poly (sodium 4-styrene-sulfonate) shell having a hydrodynamic diameter of 100 nm were purchased from Chemicell GmbH (Berlin, Germany). Dichloromethane (DCM) was obtained from Merck (Darmstadt, Germany). All proteins were dissolved in pH 8.0 phosphate buffer (0.01 M) prepared from analytical grade KH_2PO_4 and K_2HPO_4. The washing solution (PBS Tween 20) consisted of pH 8.0 phosphate buffer (0.01 M), potassium chloride (0.15 M), and Tween-20 (0.05 %). Ultrapure water (18 MΩ·cm, Millipore Corporation, USA) was used for the preparation of all aqueous solutions.

Apparatus

Electrochemical polymerization was performed in a 200 μL cell using a 2-mm-diameter gold-disk working electrode (CH Instruments, Inc., Austin, TX, USA), a Pt counter electrode, and a Ag/AgCl reference electrode. The electrodes were connected to an Autolab Pgstat 12 potentiostat/galvanostat (Eco Chemie B.V., Utrecht, The Netherlands). The electrodes were cleaned by wet polishing in two successive steps using a laboratory-made circular polisher as well as Gamma Micropolish II deagglomerated 1.0 and 0.05 μm alumina suspension (Buehler, Lake Bluff, IL, USA), respectively.

Quantitative fluorescence intensity measurements were done with an epifluorescent microscope formed by a conventional inverted microscope (IX71 with TH4-200 halogen light source, Olympus) combined with a xenon

illuminating system (75 W, ebx75 isolated, LEJ, Jena, Germany), a fluorescent mirror unit (U-MSWB2, Olympus), a Pan Fluorite objective 20× with aperture 0.4 (Olympus), and a 7.1 Megapixel digital camera (C-7070, Olympus). The mirror unit had excitation, dichromatic mirror, and emission wavelengths as follows: 420–480, 500, and 515 nm, respectively. All fluorescent images were taken using the same camera settings (80 ISO, 4 s exposure time, 4.8 aperture).

Scanning electron microscopic imaging was performed using a SEM instrument (JEOL JSM-5500LV, JEOL, Tokyo, Japan) equipped with energy-dispersive X-ray spectroscopy (EDS). The iron content of magnetic rods and the FluidMAG-PS magnetic nanoparticles was determined by electrothermal and flame atomization atomic absorption spectrometry, respectively. The flame-AAS measurements were carried out on a Varian Techton AA6 AAS spectrometer with manual impulse nebulization adapter, air-acetylene flame with 10-cm burner at a wavelength of 248.3 nm and spectral bandwidth of 0.2 nm. The electrothermal atomization AAS measurements were performed using a Perkin-Elmer HGA-500 pyrolytic graphite furnace accommodating 10–20 μL sample volume, at a wavelength of 385.9 nm and spectral bandwidth of 0.2 nm.

Magnetic collection of the rods was tested with optical transmission experiments. The light source was a 5-mW solid-state laser diode (635 nm, DLM635/5LT, Roithner Lasertechnik, Austria) and the detector was a Si photodetector (DET-90-001, Hinds Instruments, OR, USA).

Methods

Preparation of PEDOT:PSS magnetic microrods

The imprinted and non-imprinted rods were prepared using an electrochemical template synthesis method depicted in Fig. 1. Hydrophobic track-etched PC membranes with 1-μm-diameter cylindrically shaped pores were used as sacrificial microreactors for growing the polymeric microrods involving the following succession of steps:

Electrode preparation The gold electrodes were first polished with alumina suspension and ultrasonicated in 1:1 (v/v) water:isopropanol for 5 min. After this pretreatment the electrode was rinsed with deionized water and kept in water until used. The wet PC membrane disk was placed on the electrode and fixed with a custom-made Teflon ring. For the imprinted rods the electrode-membrane assembly was incubated in 10 μL template protein solution (1 mg/mL avidin-FITC) for 30 min followed by a thorough rinsing with ultrapure water to remove the unbound proteins.

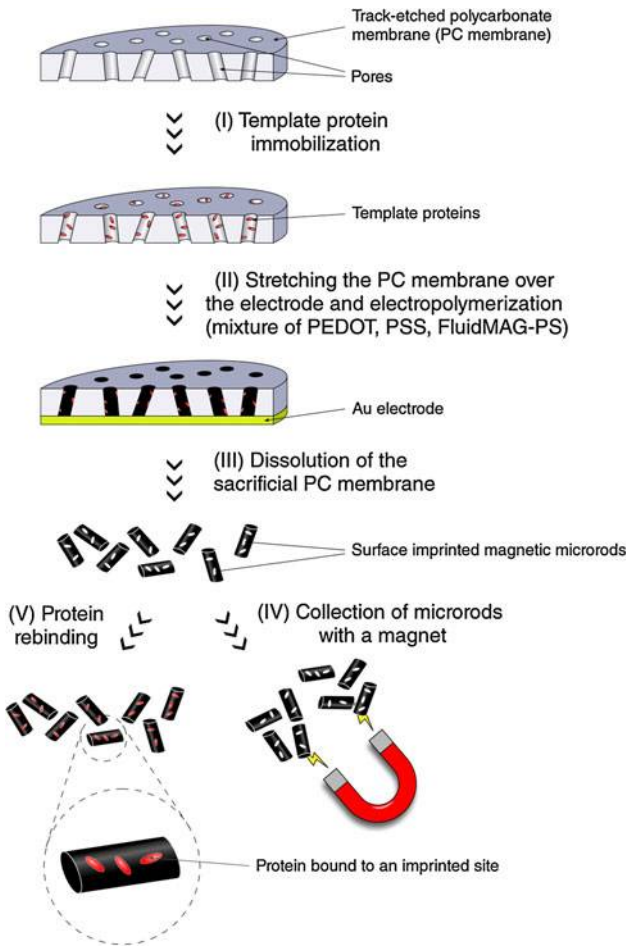

Fig. 1 Preparation of the surface-imprinted magnetic microrods using a track-etched PC membrane as a sacrificial mold

Electropolymerization After the electrodes were assembled the electrochemical cell was filled with 200 μL of deoxygenated aqueous monomer solution containing 0.01 M EDOT, 0.0125 M PSS, and 12.5 mg/mL FluidMAG-PS magnetic nanoparticles. Electrochemical synthesis of the PEDOT:PSS:FluidMAG-PS microrods was performed at constant potential ($E = 0.75$ V vs. Ag/AgCl/3 M KCl). The electropolymerization was stopped before having overgrowth of the polymer outside of the pores, i.e., when the pores were filled with the polymer composite. In the setup used this corresponded to a charge of 5 mC.

Separation of the magnetic microrods The membrane containing the synthesized microrods was first mechanically detached from the electrode surface placed in a 1.5 mL glass vial and then subjected to a series of washing and rinsing steps with the aim of extracting the magnetic

microrods. In all subsequent steps 1 mL of solvent was added to the vial containing the rods and the solution was shaken gently for 5 min. Before the solutions were removed by a micropipette the magnetic microrods were collected at the bottom of the vial for 3 min using a neodymium magnet. The extraction procedure consisted of the following successive steps: (i) incubation in 1 M NaOH for 20 min to remove excess avidin from the surface of the PC membrane and enable its dissolution in DCM, (ii) rinsing with water:methanol solution (50:50 v/v), (iii) drying the membrane, (iv) dissolving it in DCM, and (v) washing the microrods 4 times with DCM to completely remove any residual PC. Final rinses were done using a solution of methanol and water (50:50 v/v) for three times. Before the shaking steps the vial was placed in an ultrasonic bath (Realsonic 40-S, Realtrade Co., Hungary, 37 kHz nominal frequency with 350–500 V amplitude) for a few seconds to re-suspend all the rods. Also, at each separation step the successful collection of the magnetic microrods was confirmed by optical microscopy.

Epifluorescence measurements

10 μg of magnetic rods was placed in a vial with 200 μL of 10^{-2} mg/mL bovine serum albumin (BSA) to block the non-specific binding sites. After 8-min incubation the rods were separated by magnetic field from the solution, which was removed using a micropipette. The rods were washed with 200 μL aliquots of PBS Tween 20 buffer for 3 min and were collected again by a magnetic field for 2 min. To visualize the rebinding of the template avidin, the rods were incubated in avidin-FITC solutions of different concentrations, each time for 28 min followed by a 2-min magnetic separation. To remove non-specifically bound proteins, the rods were washed first with 400 μL of PBS Tween 20 and then with PB for 3 min. The collected rods were resuspended in 50 μL PB and all of them were spotted onto a glass microscope slide for imaging.

All images were taken in a dark environment using fixed settings on the epifluorescent microscope and on the camera. To evaluate the amount of bound protein, we took a fluorescence picture of the rods. The fluorescence intensity was calculated as the mean green intensity over the rods.

Determination of the iron content of the magnetic microrods and the FluidMAG-PS magnetic nanoparticles by atomic absorption spectrometry (AAS)

FluidMAG-PS nanoparticles and PEDOT:PSS polymer rods were collected by filtration on a 10-mm-diameter PVPF track-etched polycarbonate membrane filter with a pore diameter of 100 nm. The PC membrane was transferred into a small quartz crucible. 0.2 mL high-purity nitric acid (63 %) was added and then the sample was dried under an IR lamp. The crucible was placed into a furnace and ashed at 650 °C for 2 h. The residue was dissolved in 0.2 mL 1:1 mixture of cc. HNO_3 and cc. HCl and then supplemented with deionized water to a final volume of 3 mL. The iron content of FluidMAG-PS nanoparticles was determined by flame-AAS method while graphite furnace AAS method was used for the PEDOT:PSS polymer rods.

Magnetization measurement of the polymer microrods and the FluidMAG-PS magnetic nanoparticles

Magnetization measurements were carried out using a SQUID magnetometer (Magnetic Property Measurement System-Quantum Design Inc., San Diego, CA, USA). FluidMAG-PS nanoparticles and PEDOT:PSS polymer rods were collected by filtration using a PVPF track-etched polycarbonate membrane filter with a pore diameter of 100 nm. The folded membrane was placed into a gelatin-based capsule for the magnetization measurements in order to avoid the loss of polymer rods.

The diamagnetic background from the filter and the capsule were separately determined and found to be at least two orders of magnitude smaller than the signal from the sample. After the subtraction of this baseline, the magnetization curves were normalized to 1 mg magnetite (Fe_3O_4) content, as determined by AAS measurements, both in case of the FluidMAG-PS nanoparticle and the PEDOT:PSS polymer rod samples.

Results and discussion

Preparation of surface-imprinted magnetic microrods

Magnetic surface-imprinted polymer rods have been prepared by the modification of a protein-imprinting method introduced by our group to generate cylindrical microrods grafted on a solid electrode surface [39]. Here we used polycarbonate track-etched membranes with ca. one order of magnitude smaller diameters, i.e., membranes with uniform cylindrical pores of 1-μm diameter and 7-μm length, as a sacrificial mold for the confinement of the polymerization. This type of membrane is hydrophobic in nature; therefore, proteins can readily adsorb onto it from aqueous solutions. This offers straightforward means for simple physisorption of the target protein, avidin, without the need for multistep chemical synthesis or any pretreatment. Adsorption of avidin into the pores of the PC membrane has been verified using a fluorescence-labeled protein, avidin-FITC. The membrane was incubated with

different concentrations of the labeled avidin for 30 min. The adsorption isotherm can be seen in Fig. 2.

Monolayer coverage has been achieved at 1 mg/mL protein concentration so from further on this concentration has been used for the protein immobilization. 30-min incubation time was sufficient to saturate the surface of the hydrophobic membrane with the protein.

PEDOT:PSS has been chosen as the polymer matrix based on several considerations: (i) PEDOT:PSS is highly conductive (10 S/cm [40]); therefore, electropolymerization allows for unhindered spatially directed polymer growth in the membrane pores [41], (ii) polymerization of the EDOT monomer in the presence of PSS can be carried out in aqueous environment, which is a clear advantage when imprinting proteins, and (iii) the PEDOT:PSS matrix shows low non-specific protein adsorption [38, 39]. To impart magnetic properties to the polymer, commercially available superparamagnetic nanoparticles were mixed into the pre-polymerization solution. We have chosen Fe_3O_4 nanoparticles with a hydrodynamic diameter of 100 nm, because this is the minimum size of multidomain-core particles that are in-batch separable by an external magnetic field. Very importantly, they were pre-functionalized with poly(styrenesulfonate), the same polymer as the dopant, supposedly enhancing their encapsulation in the polymer matrix by charge compensation, i.e., the positive charge on the electrosynthesized PEDOT chains are compensated by the negatively charged magnetic nanoparticles owing to their PSS coating. The 1 μm PC membrane pore diameter has been chosen accordingly, to allow free access of the magnetic nanoparticles into the pores.

The surface-imprinted magnetic PEDOT:PSS polymer rods were electrosynthesized in the avidin-modified membrane pores using constant potential voltammetry until the pores were filled up completely with the polymer. A characteristic current transient recorded during electropolymerization is shown in Fig. 3.

The initial increase in the current density indicates the instantaneous formation of a thin layer of conducting polymer underneath the membrane on the electrode from the penetrated monomer solution [39]. When the monomers are depleted from this thin layer the growth of the polymer is confined exclusively to the pores. This corresponds to the current maximum at ca. 20 s. After this point the current is decreasing rapidly to the value determined by the diffusion-limited transport of the monomer within the pores. As the pore is gradually filled up with the electrically conductive PEDOT/PSS the diffusion path length of the monomers from the bulk solution is also shortened resulting in a close to linear increase in the current. The breakpoint observed at 260 s demarks a steeper increase of the current corresponding to the complete pore filling. If the electropolymerization is performed further the PEDOT:PSS film grows hemispherically around the pores at the solution-facing surface of the membrane. To limit the polymer growth to the pore interior the polymerization had to be stopped at the characteristic breakpoint which is revealed only if the polymerization time exceeds this value. As the synthesis of the microrods has proven to be very reproducible in terms of the electrical charge required to fill up the pores, the polymerization in each synthesis cycle was stopped at 5 mC. After completing the polymerization

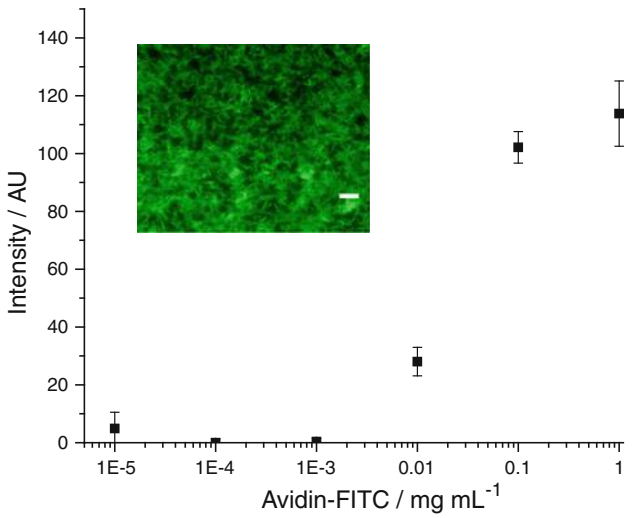

Fig. 2 Avidin-FITC adsorption on the surface of polycarbonate membrane from different concentration solutions. The *inset* shows the fluorescent microscope image of the PC membrane incubated with 0.1 mg/mL avidin-FITC. The *bar in the inset* corresponds to 10 μm

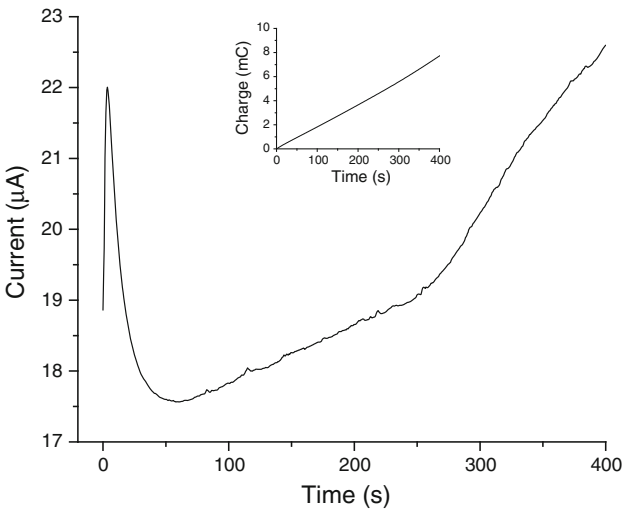

Fig. 3 Current transient recorded during the electropolymerization of a mixture of 0.01 M EDOT, 0.0125 M PSS, and 12.5 mg/mL FluidMAG-PS in the pores of a PC membrane having an adsorbed layer of avidin on the pore walls. The *inset* shows the charge versus time during polymerization

the membrane was detached from the gold electrode surface and the polycarbonate membrane was dissolved in dichloromethane. This was followed by sequential washing steps to remove the organic solvent and reconstitute the microrods in water. Washing was done batchwise, collecting the magnetic particles using a magnetic separator, aspirating the liquid, and reconstituting the particles in the next solvent by ultrasonication for 3 s. Finally, the surface-imprinted magnetic particles were obtained as dispersion in aqueous phase which facilitates their use in applications where biological antibodies might otherwise be utilized. Non-imprinted magnetic nanoparticles for comparison have also been fabricated without adsorbing avidin onto the PC membrane beforehand.

Morphological characterization of the magnetic microrods by optical and scanning electron microscopy

Optical microscope images of the particles were taken showing mostly separate, dispersed rods, including some aggregates (Fig. 4).

Taking a closer look at the microrods with scanning electron microscope revealed that many of these aggregates are, in fact, partially fused polymer particles which are formed due to the intercrossing pores in the PC membrane (Fig. 5).

There is no distinct difference at the magnification used for inspection between the surface morphology of non-imprinted and surface-imprinted particles. The microrods have relatively high aspect ratio as determined by the geometry of the PC mold, i. e., their diameter is approx. 1 μm, equal to the pore diameter, while their length is around 7 μm, equal to the thickness of the membrane. They are robust as we found that they withstand short ultrasonication without breaking apart.

Encapsulation efficiency of FluidMAG-PS magnetic nanoparticles into the magnetic microrods

We hypothesized that the charge compensation mechanism will result in an efficient incorporation of the PSS-coated magnetic nanoparticle. To find out the encapsulation efficiency we determined the iron content of the magnetic microrods as this can only originate from the magnetite content of the incorporated magnetic nanoparticles. AAS measurements revealed that the FluidMAG-PS magnetic nanoparticles contained approx. 44 % w/w iron in the form of magnetite, while the iron content of the magnetic microrods was ca. 5.1 % w/w. This implies that the FluidMAG-PS content of the magnetic polymer rods is approximately 12 % w/w. The initial polymerization mixture contains 79 % w/w magnetic nanoparticle besides the EDOT monomer (5 % w/w) and the PSS (16 % w/w). This means that the polymer rods contain roughly 6.5 times less magnetic nanoparticles than the polymerization mixture. The reason for this is related with the competition between the two negatively charged species, PSS and FluidMAG-PS, to compensate in situ the positive charge of PEDOT chains formed during electropolymerization. However, the diffusion of the much larger size FluidMAG-PS within the pores is obviously slower than that of free PSS. The diffusion coefficient of FluidMAG-PS is estimated to be 2.5×10^{-8} cm^2/s using the Stokes–Einstein equation while that of PSS is 5×10^{-6} cm^2/s [42]. While increasing the FluidMAG-PS/PSS ratio in the polymerization could have increased the amount of magnetic nanoparticles incorporated in the polymer microrods, this was unnecessary since the magnetic separability of the rods was adequate with this composition too. Of note, preliminary experiments shown that higher FluidMAG-PS content considerably decreased the rate of polymer growth while lower FluidMAG-PS/PSS ratio (0.025 M PSS vs. 2.5 mg/mL

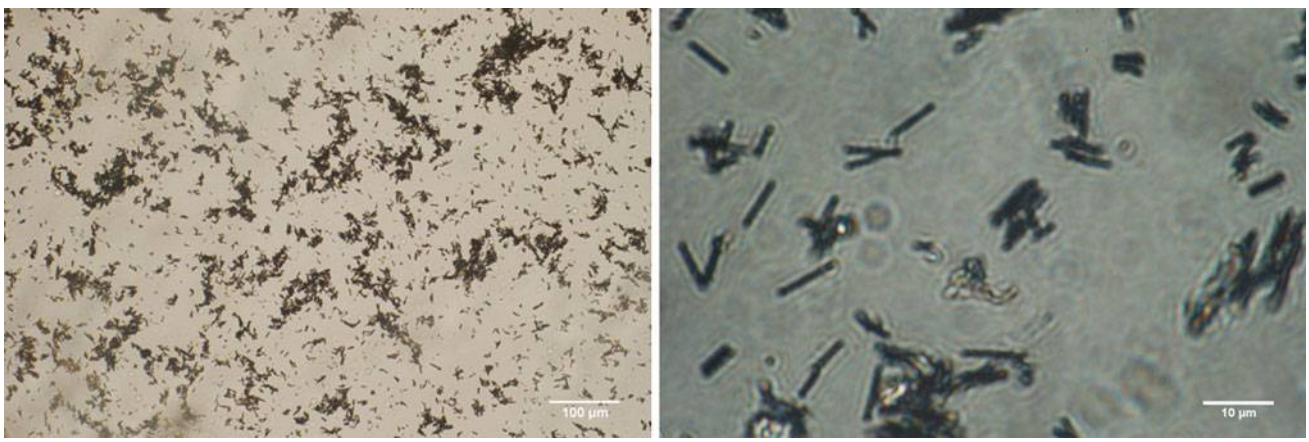

Fig. 4 Optical microscope images of surface-imprinted magnetic microrods at different magnifications

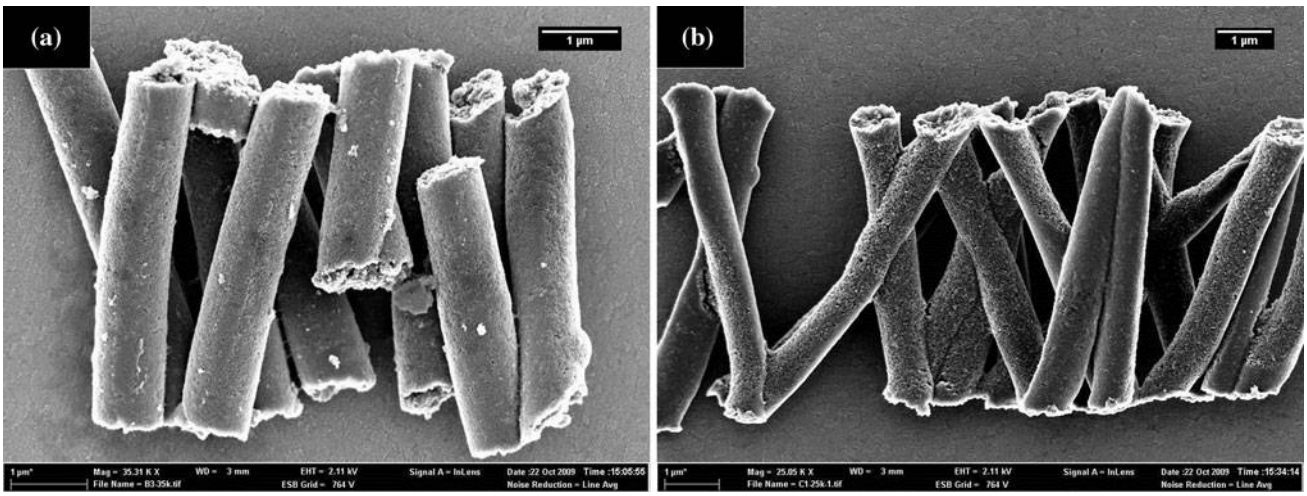

Fig. 5 Typical SEM images of non-imprinted **a** and surface-imprinted **b** magnetic PEDOT:PSS microrods. (Note that the magnifications are slightly different)

FluidMAG-PS) resulted in rods that were not magnetic enough to be collected efficiently within a reasonable time.

Magnetic properties of the magnetic polymer rods

The main goal of the measurements described below was to verify that the FluidMAG-PS magnetic nanoparticles incorporated in the polymer rods transmit their magnetic properties to the microrods thus enabling the efficient magnetic collection and separation of the polymer particles.

Magnetic properties of the FluidMAG-PS nanoparticles and microrod samples were characterized by two methods. The field dependence of their magnetization (M–H curve) was measured at room temperature with a superconducting quantum interference device (SQUID). The feasibility of magnetic collection of the rods from dilute suspensions using a permanent (NdFeB) magnet was demonstrated in routine assay conditions by optical transmission measurements.

The corresponding magnetization curves of the Fluid-MAG-PS nanoparticles and microrod samples are shown in Fig. 6. For both types of samples, the magnetization curves show superparamagnetic behavior at room temperature. No remanent magnetization is observed within the precision of the measurement when the M-H curve is recorded with decreasing magnetic field. For both types of samples a fast saturation of the magnetization is observed in the field range of 2–4 kOe (0.2–0.4 T). According to these results the magnetic properties of the magnetic nanoparticles remain intact during the polymerization. The difference observed between the magnetization of the two batches of rod samples dominantly originates from the error in the determination of their magnetite content. These results also support the reproducibility of our method for the synthesis of rods with high magnetic nanoparticle content.

As described in the previous section, the polymerized microrod samples containing magnetic nanoparticles show superparamagnetic properties with a low field of saturation, which opens a way for their magnetic collection similar to conventional magnetic nanoparticles [43]. To confirm and quantify this separation process we carried out optical transmission measurements at $\lambda = 635$ nm using a red laser as illumination source on a suspended PEDOT:PSS microrod sample containing 0.3 mg/mL microrod in water:methanol mixture (50:50 v/v). Initially the suspension

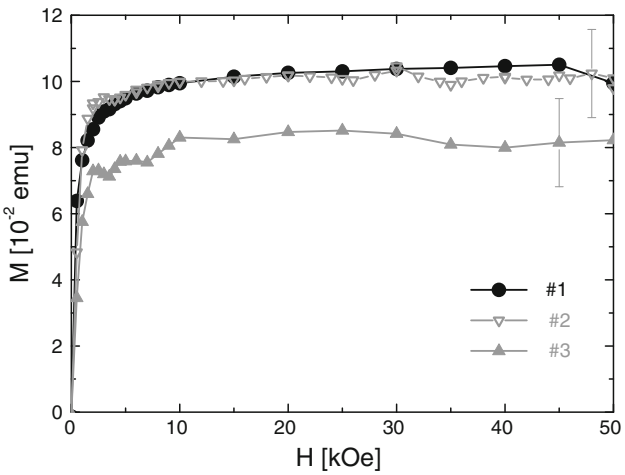

Fig. 6 Magnetization curves of the FluidMAG-PS nanoparticles (curve#1) and the PEDOT:PSS microrod samples (two independent batches: curve #2 and #3) normalized to 1 mg quantity. (The *error bars* for the microrod samples are mostly related to the uncertainty of the magnetite content determination. The reproducibility of the magnetization measurement introduces negligible error)

was ultrasonicated for 1 min to avoid the aggregation of the microrods. The light path length within the suspension was 3 mm. During the magnetic collection process we recorded the transmitted light intensity change in time, as a measure of the particle concentration, while carrying out the following steps: (i) the microrod suspension was stirred using a micropipette, and (ii) after the swirling ceased (100 s) a NdFeB rod magnet was placed near the cuvette generating a magnetic field perpendicular to the incident light beam. Movement of the magnet was carried out by a linear translation stage which ensured the precise and quick positioning, thus the transition period between the zero- and finite-field states was limited to ~ 1 s. Time dependence of the transmission upon the magnetic collection is shown in Fig. 7 where the different curves correspond to different magnet positions i.e., different magnetic fields (see Table 1), while the inset shows the zero magnetic field case, where the subsidence caused by gravity can be observed.

As shown in Fig. 7, the transmission increases exponentially after the application of magnetic field (indicated as $t = 0$ s in Fig. 7) and approaches the level of 100 % corresponding to the transmission of the water filled sample cell without the microrods. In this timeframe the measured transmission can be fitted well with the formula $T = 1-c\cdot\exp(-t/\tau)$, where c is the reduction of the transmission in the zero-field initial state due to light absorption and scattering of the rods (being proportional to the rod concentration) and $\tau$is the time constant of the magnetic collection. Thus, the density of beads in the suspension

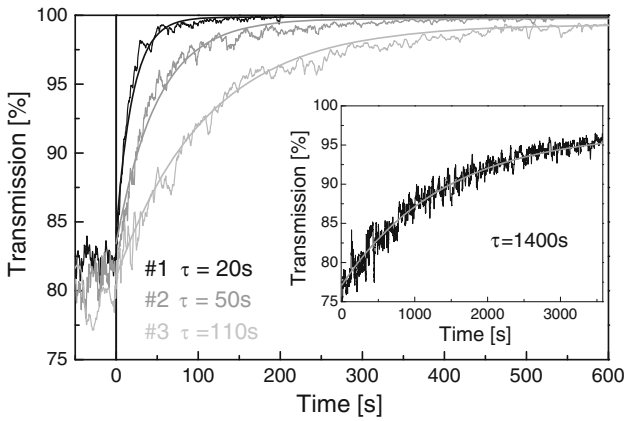

Fig. 7 Temporal dependence of the light transmission in aqueous PEDOT:PSS microrod suspensions in static magnetic fields used to collect the rods from the suspensions. The *different curves* (#1, #2, and #3) correspond to different strengths of the magnetic field as summarized in Table 1. Insertion of the magnet corresponds to $t = 0$ s. The results of fitting with exponential decay according to the formula $T = 1-c\cdot\exp(-t/\tau)$ are also indicated by *dashed lines* for each curve in the graph together with the corresponding values of the relaxation time, τ. The *inset* shows time dependence of the light transmission measured without magnetic field (curve #4)

Table 1 Time constants of the magnetic collection measurement at different distances from the magnet. Labels #1-#4 correspond to those used in Fig. 7

	Magnet position[a] [cm]	H[b] [kOe]	∂H/∂r[c] [kOe/cm]	τ[d] [s]
#1	0.5	3.18	3.8	20
#2	1.1	1.62	1.6	50
#3	2.3	0.54	0.4	110
#4	Infinity	0	0	1385

[a] Distance between the pole of the rod-shaped magnet and the light spot

[b] Strength of the magnetic field

[c] Spatial derivative of the magnetic field (along the axial direction) at the light spot

[d] The corresponding time constants of the magnetic collection measurements

exponentially decreases in time during the magnetic collection. The time constants determined by the fitting for different positions of the magnet are listed in Table 1.

Changing the position of the magnet varies the strength of the magnetic field at the location of the light spot and accordingly the magnetization of the microrods. Hence, the magnetic force acting on the microrods, (i.e., $F = \mu_0\nabla(m \cdot H)$, where μ_0 is the permeability of vacuum and m is the magnetic dipole moment of a rod), can be efficiently controlled along with the timescale of the magnetic separation. In the field range of our study the relaxation time was found to be inversely proportional to the magnetic force. As can be seen in Table 1 the rod-like NdFeB magnet used in the present study generates a magnetic field with a relatively slow spatial variation. Scaling up of the magnetic force by an order of magnitude can be easily achieved using optimally shaped magnets or by arrangements based on several permanent magnets, which makes such magnetic separation efficient for rods with considerably lower level of magnetic nanoparticle content as well.

One can observe in Fig. 7a relatively high noise at an early stage of the experiments which decays with longer times. This is due to the fluctuation caused by the rods moving in or out of focus in the very small focal spot size (10–100 μm) of the light beam. The noise is gradually reduced in time as the rods get collected by the magnet, i.e., cleared away from the detection volume. Similar reduction of noise occurs during sedimentation by gravity.

Selective binding of avidin on the surface-imprinted magnetic microrods

The existence of selective protein binding sites on magnetic avidin-imprinted PEDOT:PSS microrods has been

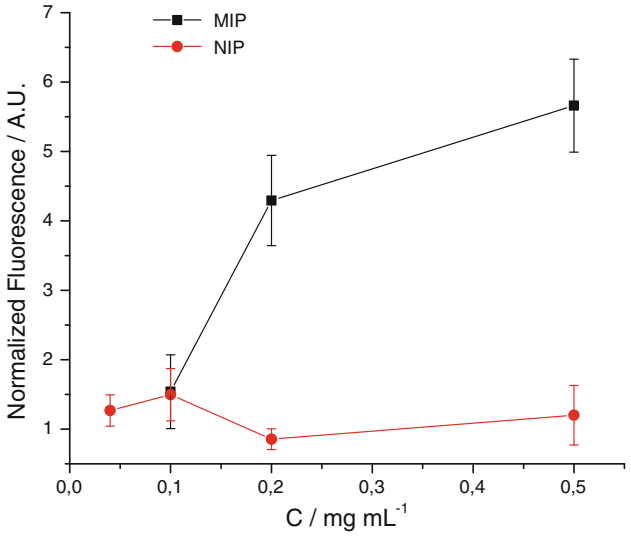

Fig. 8 Binding curve of avidin-FITC on the non-imprinted and avidin-imprinted PEDOT:PSS microrods (the *error bars* indicate the repeatability of 3 replicate measurements on the same sample)

verified by measuring the adsorption isotherm of avidin-FITC on both the imprinted and non-imprinted polymer. The microrods were incubated with different concentrations of the template protein, washed, and visualized by a fluorescence microscope. Fluorescence intensity of the particles was calculated and plotted against the concentration of the incubating solution. Fig. 8 shows the binding isotherms of non-imprinted and surface-imprinted microparticles.

As can be seen from the experiment the amount of the template protein bound by the imprinted microrods far exceeds that of the non-imprinted rods. The microrods prepared in the presence of the target protein bind approximately 5 times more avidin than the non-imprinted ones indicating the success of the imprinting process to create selective recognition sites on the polymer surface. This difference between imprinted and non-imprinted polymer is substantially higher than what was achieved in a similar approach that used wide-pore silica beads as sacrificial microreactors and free-radical crosslinking polymerization for surface imprinting of proteins [44].

Conclusion

For the first time, we have synthesized micron-sized surface-imprinted magnetic particles, by the template polymerization method, that are able to selectively capture a target protein from the sample solution. PEDOT:PSS microrods containing superparamagnetic nanoparticles were generated by electropolymerization in uniform cylindrical pores of a track-etched polycarbonate membrane, the walls of which had been modified with the target protein—avidin by simple physical adsorption. Dissolution of the membrane resulted in a suspension of micrometer-size polymer rods with selective avidin binding sites on their surface. Magnetization measurements verified the successful incorporation of the magnetite nanoparticles. The results showed that they can be collected efficiently from solution using permanent magnets employed in classical magnetic nanoparticle assays and can be redispersed afterward. This is an advantage in ligand binding assays where the surface-imprinted microrods can serve as antibody substitutes. As a proof of concept the applicability of the PEDOT:PSS microrods for the selective binding of avidin has been verified by fluorescence microscopy measurements. Due to their high specific surface area, large magnetic susceptibility, low remanent magnetization, simplicity of preparation, and high affinity toward the target protein, surface-imprinted magnetic PEDOT:PSS microrods appear to be potential candidates in binding assays, in drug delivery, and in trace enrichment of specific targets.

Acknowledgements This work is connected to the scientific program of the "Development of quality-oriented and harmonized R + D + I strategy and functional model at BME" project (TÁMOP-4.2.1/B-09/1/KMR-2010–0002). This work was supported by the European Commission (MRTN-CT-2006-033873) and Hungarian OTKA under Grant Nos. PD75615, K104724, and CNK80991. The authors would like to thank Dr. László Ferenc Kiss for the assistance during the magnetization measurements and Prof. László Bezúr for the atomic absorption measurements.

References

1. Sellergren B (ed) (2001) Molecularly imprinted polymers: Man-made mimics of antibodies and their applications in analytical chemistry. Techniques and Instrumentation in Analytical Chemistry, vol 23. Elsevier, Amsterdam
2. Komiyama M, Takeuchi T, Mukawa T, Asanuma H (2003) Molecular imprinting from fundamentals to applications. Wiley, Weinheim
3. Yan M, Ramström O (eds) (2005) Molecularly imprinted materials: science and technology. Marcel Dekker, New York
4. Haupt K (ed) (2012) Molecular imprinting. topics in current chemistry, vol 325. Springer, New York
5. Pichon V (2007) J Chromatogr A 1152:41. doi:10.1016/j.chroma.2007.02.109
6. Toth B, Horvai G (2012) Chromatography, solid-phase extraction, and capillary electrochromatography with MIPs. In: Haupt K (ed) Molecular imprinting. Topics in current chemistry, vol 325. pp 267. doi:10.1007/128_2010_100
7. Resmini M (2012) Anal Bioanal Chem 402:3021. doi:10.1007/s00216-011-5671-2
8. Holthoff EL, Bright FV (2007) Anal Chim Acta 594:147. doi:10.1016/j.aca.2007.05.044
9. Moreno-Bondi MC, Navarro-Villoslada F, Benito-Pena E, Urraca JL (2008) Curr Anal Chem 4:316. doi:10.2174/157341108785914925
10. Suryanarayanan V, Wu CT, Ho KC (2010) Electroanalysis 22:1795. doi:10.1002/elan.200900616

11. Kryscio DR, Peppas NA (2012) Acta Biomater 8:461. doi:10.1016/j.actbio.2011.11.005
12. Chen LG, Li B (2012) Anal Methods 4:2613. doi:10.1039/c2ay25354b
13. Ansell RJ, Mosbach K (1998) Analyst 123:1611. doi:10.1039/A801903G
14. Chen LG, Liu J, Zeng QL, Wang H, Yu AM, Zhang HQ, Ding L (2009) J Chromatogr A 1216:3710. doi:10.1016/j.chroma.2009.02.044
15. Chen LG, Zhang XP, Sun L, Xu Y, Zeng QL, Wang H, Xu HY, Yu AM, Zhang HQ, Ding L (2009) J Agric Food Chem 57:10073. doi:10.1021/jf902257d
16. Chen LG, Zhang XP, Xu Y, Du XB, Sun X, Sun L, Wang H, Zhao Q, Yu AM, Zhang HQ, Ding L (2010) Anal Chim Acta 662:31. doi:10.1016/j.aca.2010.01.001
17. Gu XH, Xu R, Yuan GL, Lu H, Gu BR, Xie HP (2010) Anal Chim Acta 675:64. doi:10.1016/j.aca.2010.06.033
18. Guo WL, Hu W, Pan JM, Zhou HC, Guan W, Wang X, Dai JD, Xu LC (2011) Chem Eng J (Lausanne) 171:603. doi:10.1016/j.cej.2011.04.036
19. Ji YS, Yin JJ, Xu ZG, Zhao CD, Huang HY, Zhang HX, Wang CM (2009) Anal Bioanal Chem 395:1125. doi:10.1007/s00216-009-3020-5
20. Hoogvliet JC, Dijksma M, Kamp B, van Bennekom WP (2000) Anal Chem 72:2016. doi:10.1021/ac991215y
21. Lu SL, Cheng GX, Zhang HG, Pang XS (2006) J Appl Polym Sci 99:3241. doi:10.1002/app.22997
22. Pan JM, Hu W, Dai XH, Guan W, Zou XH, Wang X, Huo PW, Yan YS (2011) J Mater Chem 21:15741. doi:10.1039/c1jm12099a
23. Pan JM, Yao H, Xu LC, Ou HX, Huo PW, Li XX, Yan YS (2011) J Phys Chem C 115:5440. doi:10.1021/jp111120x
24. Wang XB, Ding XB, Zheng ZH, Hu XH, Cheng X, Peng YX (2006) Macromol Rapid Commun 27:1180. doi:10.1002/marc.200600211
25. Zhang XP, Chen LG, Xu Y, Wang H, Zeng QL, Zhao Q, Ren NQ, Ding L (2010) J Chromatogr, B: Anal Technol Biomed Life Sci 878:3421. doi:10.1016/j.jchromb.2010.10.030
26. Zhang Y, Liu RJ, Hu YL, Li G (2009) Anal Chem 81:967. doi:10.1021/ac8018262
27. Medina-Castillo AL, Mistlberger G, Fernandez-Sanchez JF, Segura-Carretero A, Klimant I, Fernandez-Gutierrez A (2010) Macromolecules 43:55. doi:10.1021/ma902095s
28. Gai QQ, Qu F, Liu ZJ, Dai RJ, Zhang YK (2010) J Chromatogr A 1217:5035. doi:10.1016/j.chroma.2010.06.001
29. Gai QQ, Qu F, Zhang T, Zhang YK (2011) J Chromatogr A 1218:3489. doi:10.1016/j.chroma.2011.03.069
30. Kan XW, Zhao Q, Shao DL, Geng Z, Wang ZL, Zhu JJ (2010) J Phys Chem B 114:3999. doi:10.1021/jp910060c
31. Li L, He XW, Chen LX, Zhang YK (2009) Chem–Asian J 4:286. doi:10.1002/asia.200800300
32. Li L, He XW, Chen LX, Zhang YK (2009) Sci China. Ser B: Chem 52:1402. doi:10.1007/s11426-009-0182-0
33. Liu JZ, Wang WZ, Xie YF, Huang YY, Liu YL, Liu XJ, Zhao R, Liu GQ, Chen Y (2011) J Mater Chem 21:9232. doi:10.1039/c1jm10227c
34. Qu P, Lei JP, Zhang L, Ouyang RZ, Ju HX (2010) J Chromatogr A 1217:6115. doi:10.1016/j.chroma.2010.07.063
35. Wang X, Wang L, He X, Zhang Y, Chen L (2009) Talanta 78:327. doi:10.1016/j.talanta.2008.11.024
36. Zhou WH, Lu CH, Guo XC, Chen FR, Yang HH, Wang XR (2010) J Mater Chem 20:880. doi:10.1039/b916619j
37. Gao RX, Kong X, Wang X, He XW, Chen LX, Zhang YK (2011) J Mater Chem 21:17863. doi:10.1039/c1jm12414e
38. Lautner G, Kaev J, Reut J, Opik A, Rappich J, Syritski V, Gyurcsanyi RE (2011) Adv Funct Mater 21:591. doi:10.1002/adfm.201001753
39. Menaker A, Syritski V, Reut J, Opik A, Horvath V, Gyurcsanyi RE (2009) Adv Mater 21:2271. doi:10.1002/adma.200803597
40. Groenendaal BL, Jonas F, Freitag D, Pielartzik H, Reynolds JR (2000) Adv Mater 12:481. doi:10.1002/(SICI)1521-4095(200004)12:7<481:AID-ADMA481>3.0.CO;2-C
41. Martin CR (1994) Science 266:1961. doi:10.1126/science.266.5193.1961
42. Sedlak M (2001) In: Radeva T (ed) Physical chemistry of polyelectrolytes. Surfactant science series, vol 99. Marcel Dekker New York pp 1
43. Philippova O, Barabanova A, Molchanov V, Khokhlov A (2011) Eur Polym J 47:542. doi:10.1016/j.eurpolymj.2010.11.006
44. Nematollahzadeh A, Sun W, Aureliano CSA, Lutkemeyer D, Stute J, Abdekhodaie MJ, Shojaei A, Sellergren B (2011) Angew Chem. Int Ed 50:495. doi:10.1002/anie.201004774